A Facile Route towards Large Area Self-Assembled Nanoscale Silver Film Morphologies and their Applications towards Metal Enhanced Fluorescence

Erik Hohenberger[1], Nathan Freitag[1], Daniel Rosenmann[2], Venumadhav Korampally[1,3]

[1] Department of Electrical Engineering, Northern Illinois University, 340 Engineering Building, Dekalb, IL 60115, USA
[2] Center for Nanoscale Materials, Argonne National Laboratory, 9700 S. Cass Avenue, Lemont, IL 60439, USA
[3] Corresponding Author

Email: vkorampally@niu.edu

Keywords: Optical sensor; Surface plasmon resonance; Metal enhanced fluorescence; Nanofabrication; Self assembly

Abstract

We present a facile method for fabricating nanostructured silver films containing a high density of nanoscopic gap features through a surface directed phenomenon utilizing nanoporous scaffolds rather than through traditional lithographic patterning processes. This method enables tunability of the silver film growth by simply adjusting the formulation and processing conditions of the nanoporous film prior to metallization. We further demonstrate that this process can produce nanoscopic gaps in thick (100 nm) silver films supporting localized surface plasmon resonance with large field amplification within the gaps while enabling launching of propagating surface plasmons within the silver grains. These enhanced fields provide metal enhanced fluorescence with enhancement factors as high as 21 times compared to glass, as well as enable visualization of single fluorophore emission. This work provides a low-cost rapid approach for producing novel nanostructures capable of broadband fluorescence amplification, with potential applications including plasmonic and fluorescence based optical sensing and imaging applications.

I. Introduction

The past decade has witnessed an intense growth in research activities in developing surfaces and materials which can interact with light in novel ways and that could pave way towards the next generation of imaging, communication, and sensor technologies [1]–[7]. Of particular interest is in the field of plasmonics which deals with electron charge oscillations in materials, particularly metals, and the means to drive the oscillation through resonant coupling with light [8]. Noble metals have been a popular choice of material as the plasmon frequencies of these metals fall in the UV-visible-near infrared range (terahertz frequencies). Under the right coupling conditions, these materials have been shown to support surface plasmon resonance, allowing optical fields to be confined on their surfaces with large field amplifications that decay evanescently away from the surface within a few hundred nanometers [9]. This makes them useful for optical applications such as for optical waveguides, enhancing photon emission of emitting materials for sensing schemes, solar energy collection, etc. [10]–[15]

Very low roughness metallic surface boundaries can be used for supporting and manipulating propagating surface plasmons that are exquisitely dependent on the dielectric properties of the surrounding dielectric. For these structures, direct free-space coupling of light to the surface plasmons cannot be made, requiring the use of prism coupling in the Kretschmann and Otto configurations to satisfy the wave vector matching conditions [16]–[18]. Nonetheless, these SPR configurations are now widely adopted in the life sciences and sensing fields for the study of biomolecule interactions.

Free space coupling of light to metallic structures to establish propagating plasmons requires the use of surface corrugations on the metallic surface that would provide additional optical momentum matching conditions to the incoming light [19]. Such structures, typically fabricated as gratings with a well characterized grating pitch are particularly advantageous as the free space excitation of the plasmons could be accomplished through the use of inexpensive and easily available optical microscopes without the need for any additional precision optics [20], [21]. We have previously reported that such gratings architectures may indeed be replicated inexpensively from commercially available HD-DVDs or Blu-Ray discs and demonstrated the application of such structures for surface plasmon enhanced fluorescence emission [21].

Localized surface plasmons are those that are tightly bound to discrete metallic nanostructures such as nanoparticles, nanowires and also within nanoscopic metallic gaps. Metallic bow-tie configurations, nanoparticle dimers featuring sub-10 nm gaps are some of the most widely studied architectures and have been primarily been demonstrated for applications in Surface Enhanced Raman spectroscopy (SERS) and Fluorescence enhancement. Furthermore, it has been shown that the combination of discrete nanostructures that have the capability of supporting localized surface plasmon resonance with those structures that support propagating plasmons could be very advantageous leading to very large field enhancements within the structures. We have previously shown that grating coupled surface plasmon resonant structures featuring nanoscopic gaps would lead to large field intensity enhancements within those nanoscopic gaps, with enhancement factors as high as ~23 times compared to those on a flat metal surface [21]. However, such nanogaps were only intermittently present over the grating structure leading to only a few isolated hotspots across the entire surface.

To that end, we present our work towards fabricating high density submicron and nanoscale metal film grains separated by high aspect ratio nanoscopic gaps using a highly scalable and tunable fabrication scheme. Here, we rely on the use of large surface area, low surface energy nanoporous organosilicate (NPO) thin films grown on silicon substrates as a scaffold promoting dewetting of thin metallic films of elemental silver as they are being deposited upon these structures. Controlled growth of such metal islands separated with nanoscopic gaps in high densities led to large and uniform field enhancements across the entire film. The relative simplicity of fabricating the NPO films, together with the high degree of tunability these films offer, in terms of controlling the surface areas, thicknesses, surface chemistry makes this a particularly useful technique for low cost production and fine-tuning of nanogap structures.

We demonstrate that NPO films which have these nanogap structures have plasmonic properties by showcasing their ability to enhance fluorescence emission of a gain media applied over the silver film layer, and that the enhancement factor can be adjusted by simply changing the

formulation and the decomposition temperature used for the underlying NPO film. We further show that the fluorescent material applied directly over the silver film surface exhibits hot spots, the generation of very bright localized points of light emission, and blinking which is indicative of single fluorophore emission. These hot spots have unique ring patterns, which we attribute to the interference of propagating plasmons within the larger silver grain structures present on the film surface.

II. Materials and Methods

Polymethyl silsesquioxane (PMSSQ, Mw D 10 000; 14% hydroxyl groups) was obtained from Techneglas,Inc. (P/N GR650F). Polypropylene glycol (PPG, Mn: 425), Propyleneglycol methylether acetate (PGMEA, 98%), Ethanol (100% Analytical grade), were obtained from Sigma-Aldrich (St Louis, MO) and used as received. Fluorescent dye – Rhodamine 6G (R6G) was obtained from Exciton Inc.

NPO Film Formation: The general preparation strategy for the NPO film formation is described in our previously reported paper[8]. Briefly, PMSSQ and PPG were dissolved separately in the PGMEA solvent in different mass ratios. Following this, PPG solution was introduced to PMSSQ solution at different mass ratios and the resulting solutions were once again sonicated well to ensure homogenous mixing of the two solutions. Three separate solutions were prepared with the following weight ratios: 8:2 solvent (PMA) to solute, with the solute containing a ratio of 8:2 parts PPG to PMSSQ (here from referred to as 8282); 8:2 solvent to solute, with the solute containing 9:1 parts PPG to PMSSQ (here from referred to as 8291); and 5:5 solvent to solute, with the solute containing 7:3 parts PPG to PMSSQ (here from referred to as 5573). Individual solutions were spin coated onto silicon wafers at 3000rpm/30sec. Coated wafers were immediately placed onto a hot plate preheated to either 450°C or 500°C for 5 minutes. After decomposition, wafers were then air cooled to room temperature.

Optical characterization of NPO films: Optical properties of the samples were collected using a spectroscopic ellipsometry system (UVISEL Spectroscopic Ellipsometer: Horiba Jobin Yvon). Operating angle was set to 70 degrees. The incident wavelength was swept from 200 to 800 nm with a step size of 2 nm. Data was then fitted using the Cauchy Dispersion formula (A, B, and C coefficients only) to determine film thickness and refractive indices of the obtained films at 630 nm wavelength.

Silver Metallization: NPO coated wafers were metallized with silver using a PVD 250 electron beam evaporator system (Kurt J. Lesker). Vacuum pressure was held at 2×10^{-8} Torr as the base pressure for all the depositions. The substrates were rotated at 20 rpm and kept close to room temperature by means of a chilled water cooling stage, while the pressure during evaporation was maintained in the 10^{-7} Torr range or better. One set of samples were coated with Germanium adhesion layers (thickness ~ 2 nm) in the same chamber without breaking the vacuum prior to coating with silver films to examine the effect of surface preparation on the morphology of the final silver films. Depositions were done at deposition rates of 2, 10, and 30 Å/s.

Fluorescence gain medium coating: Metallized samples were coated with a fluorescent

gain medium by preparing a 1%wt. solution of PMSSQ in ethanol which was then doped with a 10uM concentration of Rhodamine 6G fluorescent dye. This solution was spin coated onto the samples at 3000rpm for 30sec. R6G was also directly deposited onto some of the sample surfaces to facilitate observation and imaging of hotspots within the samples. Dye solutions were prepared at a concentration of 1uM, 0.1uM and 0.01uM in ethanol. Samples were cut to $5mm^2$ pieces and 5uL of dye solution was dispensed over the sample pieces and allowed to air dry before fluorescence imaging.

Fluorescence imaging and characterization: Fluorescence imaging and enhancement measurements were carried out using an epifluorescence microscope (Nikon) fitted with 10x, 40x, and 100x (oil immersion) PlanFluor objectives, and equipped with a 12bit CCD high sensitivity monochrome digital camera (Hamamatsu). Excitation and emission light was filtered using a TRITC HYQ (530-560 nm Ex., 590-650 nm Em.) filter cube.

III. Results Discussion

The primary purpose of the nanoporous organosilicate films in this study was to investigate their application as a high surface area, low surface energy scaffold for the self-assembled formation of high density metallic nanogap structures within metallic films. Recent reports on such studies included the use of high density, high aspect ratio nanowires and nanorod structures that were effectively used as scaffolds to direct the metal nanogap formation and subsequent investigations through SERS enhancement studies [22]–[24]. While these studies were promising in that large field enhancements manifested as improved SERS response from these substrates were demonstrated, the fabrication of such structures and particularly the scale up of such structures are not trivial.

Here, our study investigated novel nanoporous organosilicate thin films that are essentially composed of organosilicate nanoparticles (~ 3.5 nm diameter unit particles assembling into supra-nanoparticles of *ca*. 20 nm; the high surface area arising from the inter-particle separations of the nanoparticles within the film [25], [26]. Further, the nanoparticle surface termination with methyl groups render them inert, which in combination with their nanoscale surface roughness makes them highly hydrophobic (water contact angles ~ 110^o) and with low surface energy values [26]. Therefore, these structures are particularly interesting for applications where deliberate and controlled room temperature dewetting of thin films and subsequent nanoscopic gap formation between the dewetted islands is desired.

Table 1 lists the optical characterization results of the NPO films used in this study. As can be observed, the processing temperature plays a crucial role in determining the optical properties of these films, as the formation mechanism of these films is primarily entropy driven [26]. Film properties could be further fine-tuned through controlling the formulation of the precursor solution. Because of the optically non-absorbing nature of these films, all the processed films were fitted using the Cauchy dispersion formula to obtain their thicknesses and refractive indices. In this study, refractive index has been used as an indirect metric to gauge the degree of porosity of the obtained films. Table 1 shows the sample film thickness, the A and B values for the Cauchy dispersion fitting, and the refractive index of the fitted data taken at 630 nm, and the χ^2 error parameter for the fit. The low value for the χ^2 error parameter indicates that the obtained fits were reflective of the true nature of the film. The refractive index values of the obtained

films ranged from 1.12 to 1.22 indicating that these films were inherently of low-density arising from the presence of the nanoscopic voids within the film. Predictably, higher processing temperatures yielded films with decreased refractive indices indicative of higher pore volume fraction for these films.

While increased amount of PPG within the precursor solution is expected to yield films with lower densities (lower refractive indices), 8291 films exhibited higher refractive indices than corresponding 8282 films possibly due to the very low thicknesses of these films. It is possible that the scaling of the optical properties of the films as a function of PPG concentration within the precursor formulation follows only up to a critical thickness of the final film (~ 100 nm). Nevertheless, the obtained films were porous and were used as part of this study.

Table 1. Fitted ellipsometry data for NPO films.

NPO films – processing temperature	**Thickness (Å)**	**Cauchy A**	**Cauchy B**	**n @ 630 nm**	**χ^2**
8282 - 450°C	1141.987	1.140786	0.1389235	1.144	0.015581
8282 - 500°C	1055.012	1.120835	0.1242833	1.124	0.027913
8291 - 450°C	446.104	1.217129	0.1800756	1.222	0.026744
8291 - 500°C	460.572	1.147475	0.1274224	1.151	0.014374

Control of Silver film microstructure on substrates: The growth and dynamics of microstructure formation in thin metallic films has been studied extensively in the past and significant literature on this topic exists dating back to the 1970s [27]. Dewetting of thin films, often viewed as an undesirable effect in coatings and microelectronics/microsystem fabrication, has been receiving renewed interest in the recent past. Thin film dewetting induced through substrate chemical or physical heterogeneities in combination with high temperature annealing conditions is increasingly being considered as a simple means towards patterned discrete nanoparticles or interconnected systems of nanostructures on a substrate. Often, such dewetted structures are obtained because of the inherent instabilities of the as-deposited film over the substrate. Subjecting such substrates to high temperature annealing conditions increases the mobility of the constituent atoms of the film, and driven by surface energy minimization, leads to spontaneous dewetting of the films [27]. The temperature at which dewetting proceeds is strongly correlated to the nature of the substrate as well as the thickness of the deposited films and can be much lower than the melting temperature of the metal itself.

For thin films deposited over substrates with inherently low surface energies or substrates pre-coated with self-assembled monolayers (SAM) of lubricating molecules such as methyl siloxanes, the increased mobility of the metal atoms over such surfaces leads to dewetted films even at room temperature conditions during the film deposition. An exquisite application of such dewetted thin film structures have been demonstrated by Xu *et. al.* for the fabrication of ultra-thin dewetted films of palladium for improved sensing of hydrogen [28]. Further, on physically

heterogeneous surfaces, an otherwise metastable film may be driven to instability and subsequent dewetting owing to the presence of sites with reduced local film thickness [29].

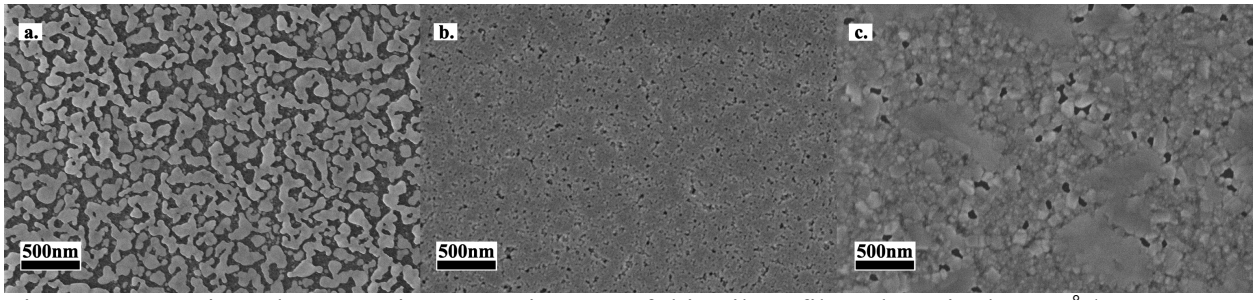

Figure 1. Scanning Electron microscope images of thin silver films deposited at 10Å/s rate over various substrates - a. NPO 8282 - 500C, b. NPO 8282 500 C with Ge adhesive layer, and c. bare Si metallized, illustrating dependence of as-deposited silver morphology on the surface functionality of the substrate.

Here, in this study, we have sought to combine the effect of low surface energy as well as nanoscale physical heterogeneity through the use of nanoporous organosilicate thin films. The low surface energy arises from the intrinsic nature of the organosilicate nanoparticles, while the nanoscopic physical heterogeneity comes from the nanoporous nature of the nanoparticulate film. Fig. 1 shows the scanning electron microscope (SEM) images of thin silver films (~ 25 nm) deposited over different substrates at a deposition rate of 10 Å/s. Silver films deposited over pristine 8282 NPO film (Fig.1a) were observed to remain in the island growth stage for the entirety of the deposition run. The silver islands (the lighter colored regions) have very discrete borders, with gap widths between individual islands ranging from a few nanometers to over 100 nanometers. On the other hand, silver films deposited over NPO films that were first coated with a thin Ge adhesion layer (~ 2 nm) as well as silver films deposited over bare silicon wafers under identical deposition conditions gave rise to starkly different film morphologies. Fig.1b and Fig. 1c shows the SEM images of silver films on Ge coated NPO film and a bare silicon wafer respectively. The silver film growth on both of these surfaces does not exhibit the same discrete island growth as was observed on the pristine NPO films, and instead resulted in a mostly featureless, mostly uniform film on the germanium coated NPO film, and grains of random size, shape, and orientation covering almost the entirety of the surface of the bare silicon wafer. The island growth stage was not maintained on these two surfaces for the entire length of the deposition run. This may be attributed to the fact that Ge and silicon are both materials with moderately high surface energies. Even with the presence of the physical heterogeneity on the NPO surfaces, the thin Ge coating essentially provided high energy defect spots that acted as anchor points for the subsequent silver atoms thereby stabilizing the film against dewetting.

Effect of processing conditions on the final Silver film morphology: Fig. 2 shows the SEM images of silver film growth on NPO films as a function of variations in processing conditions. It may be readily observed that different NPO precursor formulation were able to produce silver film islands whose conformations were unique to the NPO film they were grown on. 8282 NPO film (with an 8:2 by weight concentration of PPG to PMSSQ) processed at 450°C processing temperature resulted in Ag film with similar serpentine structures as seen in Fig. 1a. Lowering

the concentration of PPG to PMSSQ down to 7:3 by weight resulted in more uniformly shaped elliptical islands with fewer serpentine branching structures and smaller inter-island gaps. Such differences in the morphologies of the obtained structures may be solely attributed to the fine differences in the nanoscale surface roughness values as both the films are expected to possess similar surface chemical functionality due to identical processing temperatures.

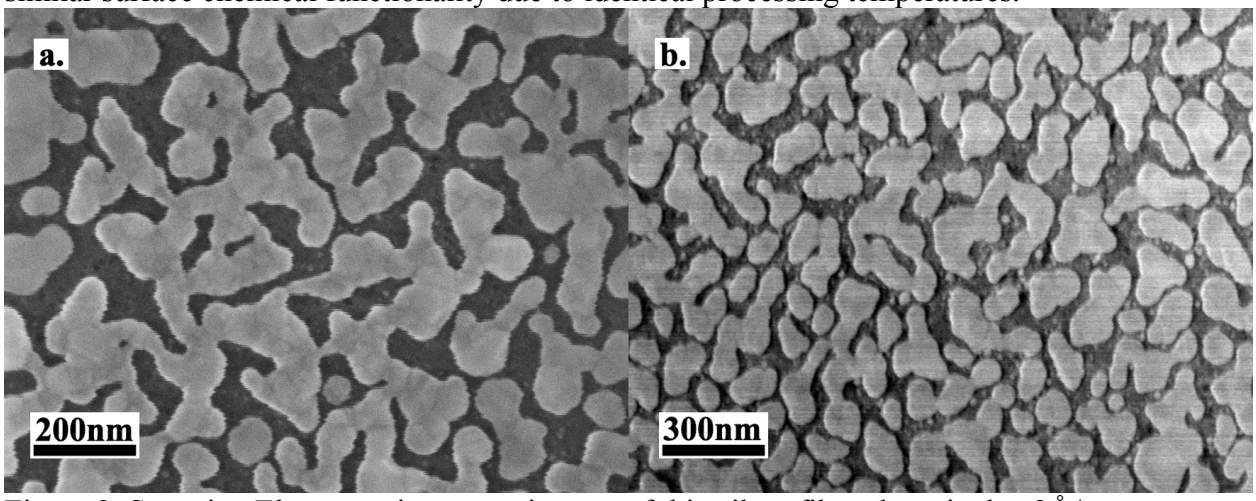

Figure 2. Scanning Electron microscope images of thin silver films deposited at 2Å/s rate over various substrates a. NPO 8282-450C and b. NPO 5573-450C, illustrating dependence of as-deposited silver morphology on the various processed NPO films.

In addition to the NPO film formulation, the processing temperature of the NPO films was also found to have a significant influence over the subsequent growth and morphology of the Ag films. It should be noted that the processing temperature while determining the final NPO film characteristics (thickness, refractive index, etc. see Table 1), also influences the surface energy of the obtained films, particularly for processing temperatures exceeding 450^{o}C. This is because, at such high temperatures, significant fraction of the organic constituents (methyl groups attached to the siloxane backbone of the nanoparticles) are removed through decomposition. It should be further noted, that, despite this removal, surface energy minimization drives the methyl groups from the bulk of the nanoparticle to its surface thereby replenishing the lost groups and maintaining the over-all low surface energy of the NPO film. Fig. 3 shows the SEM images of the silver film morphologies produced over identical NPO films but processed at two different temperatures (450°C and 500°C). 8291 films processed at 450°C and subsequent Ag deposition gave rise to a fully interconnected silver film mesh (Fig.3a), as opposed to highly branched, but discrete, serpentine structures obtained for identical films processed at 500°C (Fig.3b). Both the films were metallized in the same deposition run with total nominal thickness of Ag deposited being 25 nm deposited at 10 Å/s rate.

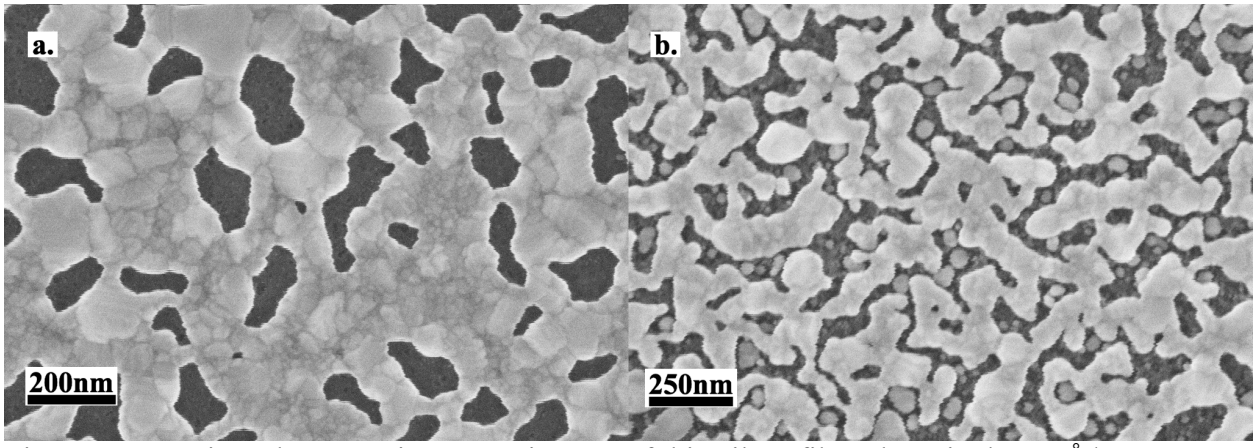

Figure 3. Scanning Electron microscope images of thin silver films deposited at 10Å/s rate over various substrates a. NPO 8291-450C and b. NPO 8291-500C, illustrating dependence of as-deposited silver morphology on the processing temperature of the NPO films.

Beyond the percolation threshold, silver films on NPO gave rise to films that were seemingly continuous. Silver films deposited to a total nominal thickness of 100 nm, exhibited Ag film morphologies consisting of submicron scale grain features separated by clearly defined gaps on the order of ≤ 30 nm wide. Because the NPO films were able to maintain the dewetted island morphologies to large thicknesses compared to bare silicon, it is reasonable to expect that the nanogaps separating the individual grains would have a higher aspect ratio compared to gaps between grains in silver films deposited on bare silicon substrates. Fig.4a and b shows the SEM images of 100 nm nominal thickness silver films deposited over NPO 8291 – 450°C film and a bare silicon wafer respectively. Depositions were specifically performed at high deposition rate of 30 Å/s to ensure the obtained silver films were composed of large grain sizes exhibiting good plasmonic properties [30].

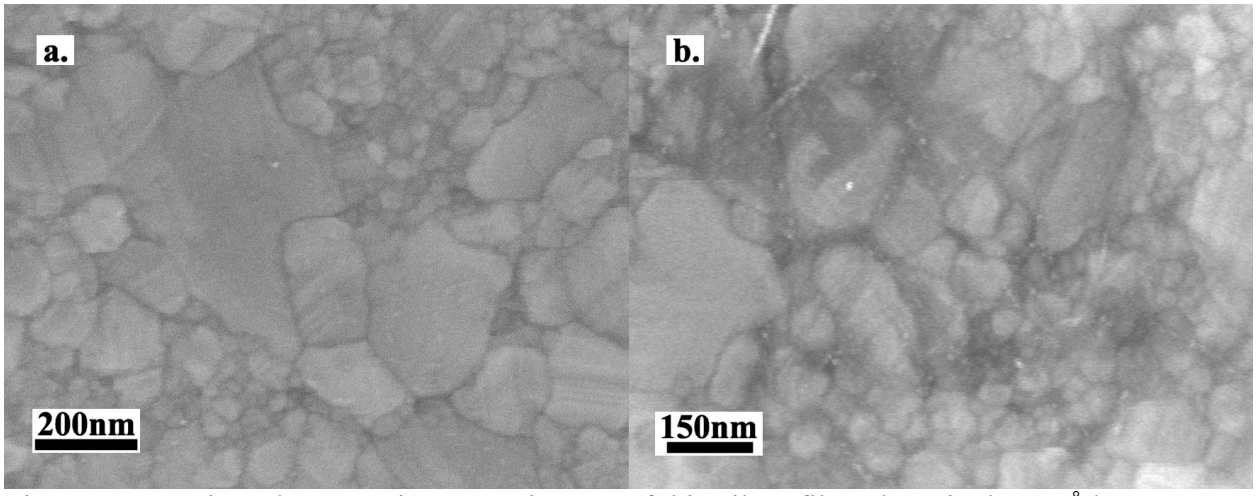

Figure 4. Scanning Electron microscope images of thin silver films deposited at 30Å/s rate over various substrates a. NPO 8291-450C and b. bare silicon, illustrating differences in the obtain silver morphologies.

Our preliminary experiments with deposition conditions and processing parameters of the NPO films indicated that the silver film morphology may indeed be appropriately tailored for specific applications. To illustrate the application of such structures, our subsequent studies were focused on investigation of metal enhanced fluorescence upon these optimized structures.

Metal enhanced fluorescence (MEF) studies: Metallic films or metallic nanoparticles and nanostructures have been known to profoundly affect the emission characteristics of fluorophores in close proximity. Large near field enhancements at surface of the metals due to Surface Plasmon Resonance (SPR) may be used to optimally excite fluorophore molecules enhancing their fluorescence emission [20], [31]–[34]. The emission characteristics of the fluorophores themselves are advantageously modulated by the presence of the metal in terms of increased quantum yields of weakly fluorescent molecules, reduced lifetimes and subsequently improved photostabilities [35]–[37]. A more quantitative description of the fluorescence rate enhancement of a fluorophore (ψ_{em}) in close proximity to a metal surface is given by

$$\psi_{em} = \chi \frac{Q^m}{Q^o},$$

where, χ is the enhancement in the excitation rate experienced by the fluorophore owing to its localization within the large near field established over the metal surface [38]. Q^o and Q^m are the quantum yields of the fluorophore excited in free space and the modified (apparent) quantum yields of the fluorophore due to the increased radiative decay rate experienced at the metal surface respectively. Note that for fluorophores with high intrinsic quantum yields ($Q^o \sim 1$), the ratio $\frac{Q^m}{Q^o}$ is approximately equal to one signifying that the fluorescence rate enhancement observed may exclusively be attributed to electromagnetic field enhancement at the structured metal surface. Such high intrinsic quantum yield fluorophores are therefore particularly suitable when investigating structures or platforms for their near field enhancement, separating this from other photo-physical effects on the fluorophores due to the presence of the metallic structures that accompanies MEF [39]. χ, the enhancement in the excitation rate experienced by the fluorophore in turn may be expressed as:

$$\chi = \frac{\left|E(x_d,\ \lambda_{ex})e_p\right|^2}{|E_i|^2}$$

where $E(x_d,\ \lambda_{ex})$ is the electric field at the surface of the metal at the position of the fluorophore location at the wavelength of excitation, e_p is the fluorophores orientation with respect to the surface plane and E_i is the electric field the fluorophore would have experienced under free space excitation conditions (in the absence of the structured metal).

Here, in this study, we sought to investigate the use of the self-assembled Ag metallic films directed by the underlying NPO surfaces for fluorescence enhancement studies. Rhodamine 6G (R6G) with a relatively high intrinsic quantum yield $Q^o \sim 0.95$ was used as the probing dye in these studies. An epifluorescence microscope fitted with a CCD camera was used to capture grey-scale images of nanogap sample surfaces. Fig. 5 shows a representative image that illustrates the fluorescence enhancement of R6G film on a glass substrate (Fig.5a), Silver

deposited over bare silicon wafer (Fig.5b) and Silver deposited over NPO 8291-450°C sample (Fig. 5c). All of these samples were coated with the silver to a nominal thickness of 100 nm, at a deposition rate of 30 Å/s. The average pixel values from these images were used to determine the fluorescence enhancement factor (EF) by selecting 3 sub-regions from each image and finding the average overall pixel value for each image. The following formula was used to determine the EF for each sample with respect to a non-metalized glass control slide:

$$EF = \frac{I_n - I_{nB}}{I_f - I_B}$$

Where I_n is the average pixel intensity of a sample coated with a fluorescent dye gain medium, I_{nB} is the background average pixel intensity of the sample without the gain medium coating, I_f is the average pixel intensity of the glass control slide coated with the gain medium, and I_B is the background average pixel intensity of the glass control slide without the gain medium coating [21]. The images of the glass control slide and the metalized bare silicon wafer were captured with a software image gain of 50 and an exposure time of 100ms. When imaging the nanogap samples at this gain and exposure, the captured images were almost completely saturated. The mean intensities for these samples were therefore found through linear extrapolation of multiple images captured at shorter, non-saturating exposure times (See Supporting information). Fig. 5c shows one of the NPO films imaged at 25ms exposure time. The intensity is comparable to the metalized bare silicon wafer in Fig 5b, which was captured with a longer exposure time.

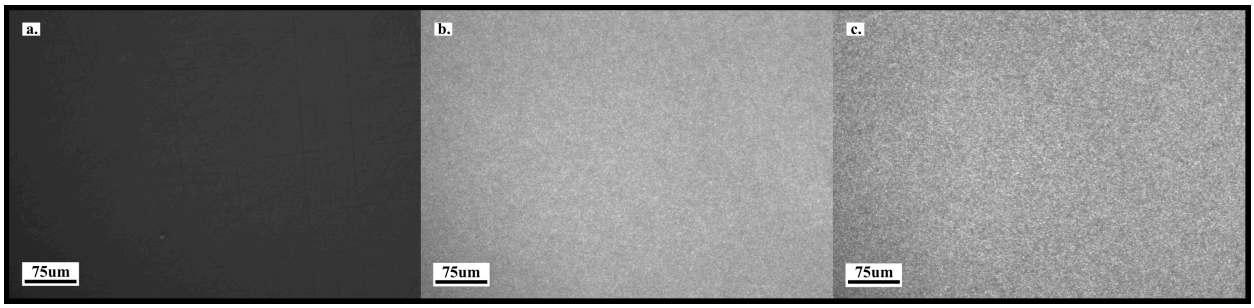

Figure 5. Epifluorescence microscope images a. untreated glass slide (100ms exposure time), b. 100 nm Ag film deposited onto bare Si substrate (100ms exposure time), c. 100 nm Ag film deposited onto NPO 8291-450C (25ms exposure time). All samples were coated with a PMSSQ film doped with R6G at a concentration of 10uM. All images were captured at 10X magnification, with a software gain of 50.

It is remarkable that even with no apparent order in the metal grain morphology obtained or the presence of precisely patterned metallic nanostructures, significant enhancement in fluorescence was obtained for Ag films on NPO. As will be shown later through our simulations and single molecule imaging study, we attribute this large enhancement to the unique nanostructuring of the Ag films, comprising of nanoscopic gaps embedded between large, flat and smooth silver grains. In addition to capable of supporting large field enhancements within the nanogaps, these nanogaps served the dual purpose of acting as slit defects that could provide for the momentum matching between the free space excitation light ($\mathbf{k_0}$) and the surface plasmons ($\mathbf{k_{sp}}$) within the silver grains [40]. Propagating plasmons within the individual silver grains establish large evanescently decaying fields that serve to amplify fluorescence from fluorophores that are not

necessary present within the nanogaps. Remarkably, despite the presence of large and smooth silver grains for silver deposited over bare silicon substrates, only modest enhancement in fluorescence was observed owing to the lack of the high aspect ratio nanoscopic gaps for these samples.

It is important to note that the obtained Ag structures directed by NPO films are particularly advantages as these could provide for broadband amplification of fluorescence emission. Such structures are especially applicable for multiplexed fluorescence based assays where multiple fluorophores with different emission wavelengths are utilized. The broadband coupling characteristics for these structures comes from the fact that these structures containing nanoscopic gaps (or slits) have Fourier Transforms that contain broadband **k** vectors and the fact that these structures with their randomly oriented grains lack any particular order. To illustrate this fact as well as to validate our hypothesis that the unique nanostructuring of the silver films establishes propagating surface plasmons across the entire substrate in addition to setting up localized and amplified fields within the nanogaps, electromagnetic field simulations were performed. Simulations were performed using Finite Difference Time Domain (FDTD) solutions of the Maxwell's equations using the commercially available software package – Lumerical Solutions. For simplicity, we had simulated single nanogaps embedded in an infinite silver film such that we could capitalize on the 2D symmetry of such a structure for faster simulation time Details of the simulation set-up and time domain simulation videos showing coupling of propagating surface plasmons to the flat regions enabled by the nanogaps for different excitation wavelengths and angles of excitation may be found in the supporting information section of this document. Such simulations consisting of different slit dimensions and orientations may be superimposed to obtain field profiles of the actual experimentally realized structures which were much more complex with presumably different slit width - depth dimensions and orientations.

A more quantitative analysis of the fluorescence enhancement over the different NPO films investigated in this study is presented in Fig. 6. The maximum fluorescence enhancement was obtained for the NPO 8291-450°C samples with the mean enhancement factor up to 21 times, compared to a glass control sample. As previously noted, the morphology of the obtained Ag films was highly dependent on the NPO precursor formulation as well as the processing temperature and this, expectedly translated to the variations in the enhancement factors obtained over each of these wafers. Decomposition temperatures at 450°C produced higher enhancements for both NPO formulations compared to counterparts decomposed at 500°C. Over all NPO – 8291 films produced higher enhancements for both decomposition temperatures compared to NPO-8282 films.

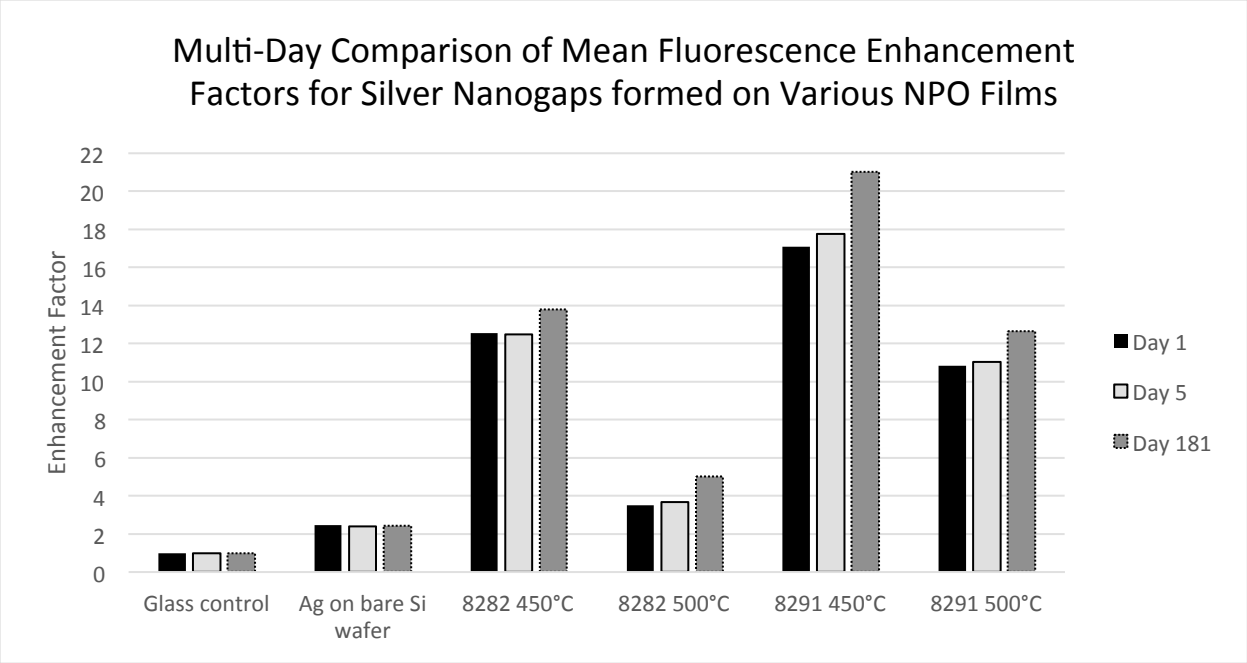

Figure 6. Mean fluorescence enhancements for various NPO films coated with 100 nm silver.

Further, we had performed a long term stability studies on these substrates as these substrates are intended to be eventually applied for sensing/diagnostic applications. Our long term stability studies indicated that the samples retained their fluorescence amplification characteristics over long term storage under less than ideal conditions (samples were stored covered in an Aluminum foil but exposed to ambient air). It may further be noticed that the over-all enhancement factor for samples stored for 180 days actually exhibited an unexpected increase in the fluorescence enhancement factor across all of the NPO films. Such an increase may possibly be due to the formation of a thin silver sulfide layer on the surface of the silver film owing to its exposure to ambient air thereby serving as a new spacer layer between the fluorophore molecules and the pristine silver surface. It is well known that fluorophore molecules that are present within 5 nm of a metal surface experience fluorescence quenching due to energy transfer to the metal. Typically to prevent quenching, spacer layers are therefore formed on the metal surfaces prior to deposition of the fluorescent layer. In our studies, the over-all fluorescence intensities obtained for each of the freshly prepared samples therefore takes into account this quenching. Remarkably, no such increase was evident for silver deposited over bare silicon wafer. This may be rationalized based on the fact that NPO films, owing to their interconnected pore structure and high surface areas offer increased avenues towards surface reactions on the Ag surface compared to the Ag films over bare (flat) silicon substrates.

Hotspots and single fluorophore emission patterns: For a more systematic study on the origin of fluorescence enhancement over the structured Ag – NPO films, single molecule studies were employed through deposition of low concentration of the R6G dyes, directly onto the Ag-NPO sample surface. Imaging such samples revealed a high density of hotspots - areas of intense electric field enhancement, appearing as discrete spots of high fluorescence intensity distributed across the entirety of the samples. These individual hotspots were resolved only at high magnification (100 X), appearing as indistinguishable bright fluorescent spots at low

magnifications. The fluorescence emission from the hot spots was further found to be intermittent which is characteristic of blinking associated with individual fluorophore emission. Owing to the strong field confinement within the nanogaps, individual fluorophore emission characteristics were observable even with a standard epi-fluorescence microscope. Fig. 7 illustrates this for the emission from a 100 nm silver deposited NPO 8291-450°C sample captured at 100 X magnification. Fig. 7a shows a representative image of the hotspot distribution at 100 X, while Fig.7b gives a zoomed in image of a single fluorophore emission captured during its 'on' time. [time-lapse videos of the actual fluorescence emission may be found in the supporting information section]. Clear and unique diffraction ring patterns were observed accompanying each fluorophore emission; the uniqueness of such patterns for different hotspots suggesting that the observed rings are not a result of an artifact of the imaging system, such as a lens flare, but rather due to the intrinsic nature of the sample itself.

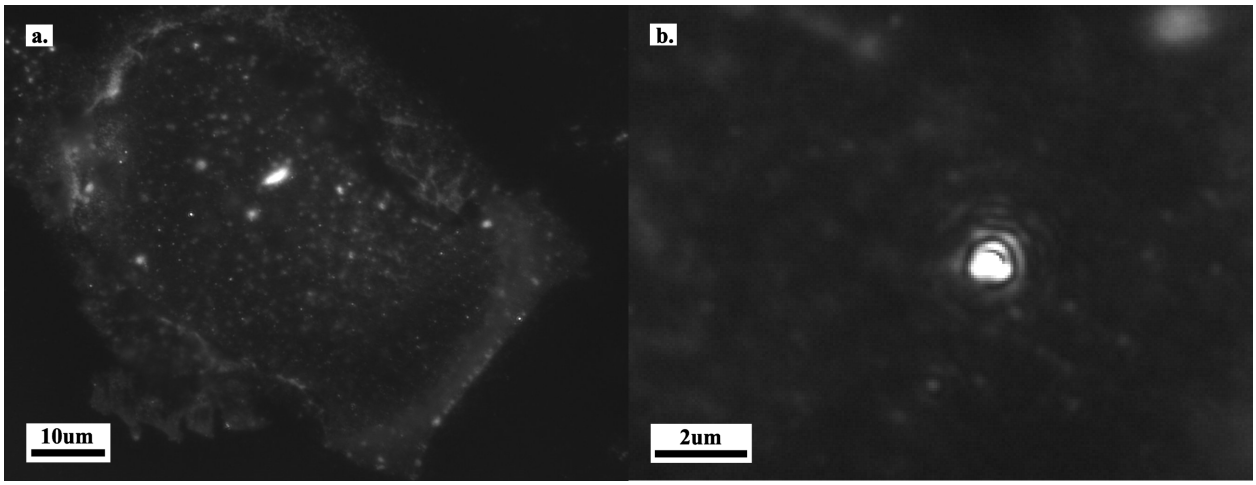

Figure 7. Epifluorescence microscope images a. dye-doped ethanol solution incubated onto 100 nm Ag deposited onto NPO 8291-450C surface, taken at 100X magnification with immersion oil b. digitally zoomed in region from a video still frame recorded using the same sample as in a. (see Supporting information for the full video). The sample substrate was cut to an area of $5mm^2$. Ethanol was doped to a concentration of 0.01uM R6G dye. 5uL of this solution was applied to the sample surface.

Single molecule imaging through fluorescence or Raman microscopy presents a simple and convenient means to the mapping of the near-field surface Plasmon fields in the far field [41]. Here, our single molecule studies essentially presented us with a means to not only study the hotspot distribution across the obtained samples but also the surface plasmon interference patterns established over the individual Ag grains from the counter propagating SP waves. Because of the lack of apparent order within the obtained structures, as well as the lack of control of the orientation of the single fluorophores within the structure, the point-spread functions accompanying individual fluorophore emissions were unique to their spatial locations. Such modulated point-spread functions of single fluorophore emitters through the use of structured plasmonic substrates are particularly of interest for super-resolution imaging applications [42].

IV. Conclusion

In conclusion, we have reported a simple and facile method of preparing structured silver films with high density of hot-spot distribution across the substrate through a simple surface driven dewetting phenomenon. High surface area, low surface energy nanoporous organosilicate films have been used as a scaffold to drive the Ag nanostructure formation during the deposition process. We have further shown that NPO films can also drive the formation of deep nanoscopic gaps between grains in thick silver island films (100 nm thickness). These nanoscopic gaps, while establishing strong field confinement within the gap areas also served as the necessary slit defects to match the surface plasmon wave vectors within the silver grains with free space excitation light, thereby supporting propagating surface plasmons over the grains. In addition to demonstrating metal enhanced fluorescence over these structures, with enhancement factors as high as 21 compared to glass, these structures were also able to distinguish single fluorophore emission characteristics. Point spread functions of the single fluorophore emission further consisted of unique diffraction ring patterns indicative of the interference between counter propagating surface plasmon waves over the silver grains. The simplicity of fabrication of such structures that doesn't require any precision patterning and that are capable of broadband fluorescence amplification are particularly applicable for the fabrication of fluorescence based optical sensors and for imaging applications.

Acknowledgements

This work was performed, in part, at the Center for Nanoscale Materials, a U.S. Department of Energy, Office of Science, Office of Basic Energy Sciences User Facility under Contract No. DE-AC02-06CH11357. The authors would like to thank Gregg Westberg at Northern Illinois University's Microelectronics Research and Development Laboratory for assistance with performing scanning electron microscopy imaging. The authors would also like to thank Ralu Nana Silvia Divan at Argonne National Laboratory's Center for Nanoscale Materials for assistance with ellipsometry and scanning electron microscopy imaging.

References

[1] M. I. Stockman, "Spasers explained," *Nat. Photonics*, vol. 2, no. 6, pp. 327–329, Jun. 2008.
[2] F. Vollmer and S. Arnold, "Whispering-gallery-mode biosensing: label-free detection down to single molecules," *Nat. Methods*, vol. 5, no. 7, pp. 591–596, Jul. 2008.
[3] H. F. Ma and T. J. Cui, "Three-dimensional broadband ground-plane cloak made of metamaterials," *Nat. Commun.*, vol. 1, no. 3, pp. 1–6, Jun. 2010.
[4] H. Szmacinski, R. Badugu, and J. R. Lakowicz, "Fabrication and characterization of planar plasmonic substrates with high fluorescence enhancement," *J. Phys. Chem. C*, vol. 114, no. 49, pp. 21142–21149, 2010.
[5] Y. Liu, S. Wang, Y.-S. Park, X. Yin, and X. Zhang, "Fluorescence enhancement by a two-dimensional dielectric annular Bragg resonant cavity," *Opt. Express*, vol. 18, no. 24, p. 25029, Nov. 2010.
[6] J. D. Ryckman, Y. Jiao, and S. M. Weiss, "Three-dimensional patterning and morphological control of porous nanomaterials by gray-scale direct imprinting," *Sci. Rep.*, vol. 3, Mar. 2013.

[7] A. Yang *et al.*, "Real-time tunable lasing from plasmonic nanocavity arrays," *Nat. Commun.*, vol. 6, Apr. 2015.
[8] J. R. Lakowicz, "Radiative decay engineering 5: metal-enhanced fluorescence and plasmon emission," *Anal. Biochem.*, vol. 337, no. 2, pp. 171–194, Feb. 2005.
[9] E. Fort and S. Grésillon, "Surface enhanced fluorescence," *J. Phys. Appl. Phys.*, vol. 41, no. 1, p. 013001, Jan. 2008.
[10] T. Ha and P. Tinnefeld, "Photophysics of Fluorescence Probes for Single Molecule Biophysics and Super-Resolution Imaging," *Annu. Rev. Phys. Chem.*, vol. 63, pp. 595–617, 2012.
[11] E. T. F. Rogers and N. I. Zheludev, "Optical super-oscillations: sub-wavelength light focusing and super-resolution imaging," *J. Opt.*, vol. 15, no. 9, p. 094008, 2013.
[12] H. Wei and H. Xu, "Nanowire-based plasmonic waveguides and devices for integrated nanophotonic circuits," *Nanophotonics*, vol. 1, no. 2, pp. 155–169, 2012.
[13] Y. Jian and V. Pol, "Nanocrosses with Highly Tunable Double Resonances for Near-Infrared Surface-Enhanced Raman Scattering," *Int. J. Opt.*, vol. 2012, p. e745982, Feb. 2012.
[14] K. R. Catchpole and A. Polman, "Plasmonic solar cells," *Opt. Express*, vol. 16, no. 26, p. 21793, Dec. 2008.
[15] H. A. Atwater and A. Polman, "Plasmonics for improved photovoltaic devices," *Nat. Mater.*, vol. 9, no. 3, pp. 205–213, Mar. 2010.
[16] E. Kretschmann and H. Raether, "Notizen: radiative decay of non radiative surface plasmons excited by light," *Z. Für Naturforschung A*, vol. 23, no. 12, pp. 2135–2136, 1968.
[17] A. Otto, "A new method for exciting non-radioactive surface plasma oscillations," *Phys Stat Sol*, vol. 26, pp. K99–K101, 1968.
[18] A. Otto, "Excitation of nonradiative surface plasma waves in silver by the method of frustrated total reflection," *Z. Für Phys.*, vol. 216, no. 4, pp. 398–410, 1968.
[19] H. Raether, "Surface plasmons on smooth surfaces," in *Surface Plasmons on Smooth and Rough Surfaces and on Gratings*, Springer Berlin Heidelberg, 1988, pp. 4–39.
[20] X. Cui, K. Tawa, H. Hori, and J. Nishii, "Tailored Plasmonic Gratings for Enhanced Fluorescence Detection and Microscopic Imaging," *Adv. Funct. Mater.*, vol. 20, no. 4, pp. 546–553, Feb. 2010.
[21] K. Bhatnagar *et al.*, "Fluorescence enhancement from nano-gap embedded plasmonic gratings by a novel fabrication technique with HD-DVD," *Nanotechnology*, vol. 23, no. 49, p. 495201, Dec. 2012.
[22] E. Galopin, J. Barbillat, Y. Coffinier, S. Szunerits, G. Patriarche, and R. Boukherroub, "Silicon Nanowires Coated with Silver Nanostructures as Ultrasensitive Interfaces for Surface-Enhanced Raman Spectroscopy," *ACS Appl. Mater. Interfaces*, vol. 1, no. 7, pp. 1396–1403, Jul. 2009.
[23] M. Becker *et al.*, "Selectively Deposited Silver Coatings on Gold-Capped Silicon Nanowires for Surface-Enhanced Raman Spectroscopy," *ChemPhysChem*, vol. 10, no. 8, pp. 1219–1224, Jun. 2009.
[24] T Qiu and X L Wu and J C Shen and Peter C T Ha and Paul K Chu, "Surface-enhanced Raman characteristics of Ag cap aggregates on silicon nanowire arrays," *Nanotechnology*, vol. 17, no. 23, p. 5769, 2006.

[25] S. Bok *et al.*, "Confeito-like assembly of organosilicate-caged fluorophores: ultrabright suprananoparticles for fluorescence imaging," *Nanotechnology*, vol. 23, no. 17, p. 175601, May 2012.
[26] V. Korampally, M. Yun, T. Rajagopalan, P. K. Dasgupta, Keshab Gangopadhyay, and S. Gangopadhyay, "Entropy driven spontaneous formation of highly porous films from polymer–nanoparticle composites," *Nanotechnology*, vol. 20, no. 42, p. 425602, 2009.
[27] C. V. Thompson, "Solid-State Dewetting of Thin Films," *Annu. Rev. Mater. Res.*, vol. 42, no. 1, pp. 399–434, 2012.
[28] T. Xu *et al.*, "Self-assembled monolayer-enhanced hydrogen sensing with ultrathin palladium films," *Appl. Phys. Lett.*, vol. 86, no. 20, p. 203104, May 2005.
[29] K. Kargupta and A. Sharma, "Dewetting of Thin Films on Periodic Physically and Chemically Patterned Surfaces," *Langmuir*, vol. 18, no. 5, pp. 1893–1903, Mar. 2002.
[30] K. M. McPeak *et al.*, "Plasmonic Films Can Easily Be Better: Rules and Recipes," *ACS Photonics*, vol. 2, no. 3, pp. 326–333, Mar. 2015.
[31] R. Bardhan, N. K. Grady, J. R. Cole, A. Joshi, and N. J. Halas, "Fluorescence Enhancement by Au Nanostructures: Nanoshells and Nanorods," *ACS Nano*, vol. 3, no. 3, pp. 744–752, Mar. 2009.
[32] O. G. Tovmachenko, C. Graf, D. J. van den Heuvel, A. van Blaaderen, and H. C. Gerritsen, "Fluorescence Enhancement by Metal-Core/Silica-Shell Nanoparticles," *Adv. Mater.*, vol. 18, no. 1, pp. 91–95, Jan. 2006.
[33] J. R. Lakowicz, "Radiative decay engineering 3. Surface plasmon-coupled directional emission," *Anal. Biochem.*, vol. 324, no. 2, pp. 153–169, Jan. 2004.
[34] D. Cheng and Q.-H. Xu, "Separation distance dependent fluorescence enhancement of fluorescein isothiocyanate by silver nanoparticles," *Chem. Commun.*, no. 3, pp. 248–250, Jan. 2007.
[35] A. Kinkhabwala, Z. Yu, S. Fan, Y. Avlasevich, K. Müllen, and W. E. Moerner, "Large single-molecule fluorescence enhancements produced by a bowtie nanoantenna," *Nat. Photonics*, vol. 3, no. 11, pp. 654–657, Nov. 2009.
[36] J. R. Lakowicz, "Radiative Decay Engineering: Biophysical and Biomedical Applications," *Anal. Biochem.*, vol. 298, no. 1, pp. 1–24, Nov. 2001.
[37] J. R. Lakowicz *et al.*, "Radiative Decay Engineering: 2. Effects of Silver Island Films on Fluorescence Intensity, Lifetimes, and Resonance Energy Transfer," *Anal. Biochem.*, vol. 301, no. 2, pp. 261–277, Feb. 2002.
[38] D. Darvill, A. Centeno, and F. Xie, "Plasmonic fluorescence enhancement by metal nanostructures: shaping the future of bionanotechnology," *Phys. Chem. Chem. Phys.*, vol. 15, no. 38, pp. 15709–15726, Sep. 2013.
[39] Q. Cui, F. He, L. Li, and H. Möhwald, "Controllable metal-enhanced fluorescence in organized films and colloidal system," *Adv. Colloid Interface Sci.*, vol. 207, pp. 164–177, May 2014.
[40] H. Ditlbacher *et al.*, "Fluorescence imaging of surface plasmon fields," *Appl. Phys. Lett.*, vol. 80, no. 3, pp. 404–406, Jan. 2002.
[41] L. Du *et al.*, "Mapping plasmonic near-field profiles and interferences by surface-enhanced Raman scattering," *Sci. Rep.*, vol. 3, Oct. 2013.
[42] F. Wei and Z. Liu, "Plasmonic Structured Illumination Microscopy," *Nano Lett.*, vol. 10, no. 7, pp. 2531–2536, Jul. 2010.

SUPPLIMENTARY INFORMATION

A Facile Route towards Large Area Self-Assembled Nanoscale Silver Film Morphologies and their Applications towards Metal Enhanced Fluorescence

Erik Hohenberger[1], Nathan Freitag[1], Daniel Rosenmann[2], Venumadhav Korampally[1,3]

[1] Department of Electrical Engineering, Northern Illinois University, 340 Engineering Building, Dekalb, IL 60115, USA
[2] Center for Nanoscale Materials, Argonne National Laboratory, 9700 S. Cass Avenue, Lemont, IL 60439, USA
[3] Corresponding Author

I. Determination of Fluorescence Enhancement Factors for Ag-NPO Samples

In order to determine the fluorescence enhancement factors for our samples, we captured greyscale digital images of our sample surfaces using a 12 bit CCD camera fitted to an epifluorescent microscope. This microscope allowed us to capture the fluorescence emission from the surface while filtering out the excitation light. The pixel values for each sample were averaged using the image measurement feature in ImageJ, freeware image analysis software provided by the National Institutes of Health, which can determine the mean grayscale value of a selected area of an image. These values from our samples were then compared to out sample, a glass slide coated with the same film gain medium as our samples (PMSSQ solution doped to a 10uM concentration of Rhodamine 6G dye).

When capturing images for our samples which contained the nanogap features, we found that the camera's detector would become fully saturated when the system was set to the same gain and exposure time as our glass control sample, resulting in a fully whited out image with the image pixels set to the maximum bit value. This prevented us from calculating correct enhancement factors for these samples because an intensity increase past the saturation point would not correspond to an increase in pixel bit value.

To remedy this, we reduced the exposure time for the nanogap samples until the captured image was no longer saturated, and then captured 5 images at different exposure times at or below this non-saturated time. For each of these 5 images, 3 areas were selected and measured to find the mean greyscale value for each area, and then all 3 values were averaged together to determine a mean pixel value for the given exposure time.

This data was then plotted in Excel (Microsoft Corp.) to find a best-fit trend line for each sample's set of 5 mean pixel values in order to perform a linear extrapolation to the correct mean pixel value for 100ms exposure time. We used Excel's built-in trend line fitting function along with the line equation and R^2 functions to determine the slope-intercept equation of the trend line and to ensure the data is fitted correctly. The extrapolated mean pixel value was then found by simply plugging the time (100ms) into the x-value for the slope-intercept equation. This value was then used in the Enhancement Factor formula as I_n, the average pixel intensity of a sample coated with fluorescent dye gain medium, to the determine the fluorescence enhancement factor

for the given sample. Figures S1-S4 below show the trend line graphs for the nanogap samples as measured on Day 1. 5 images were captured for each sample, with exposure times ranging for 5msec to 25msec, in increments of 5msec. Slope-intercept formulas and R^2 for each trend line are provided on each graph.

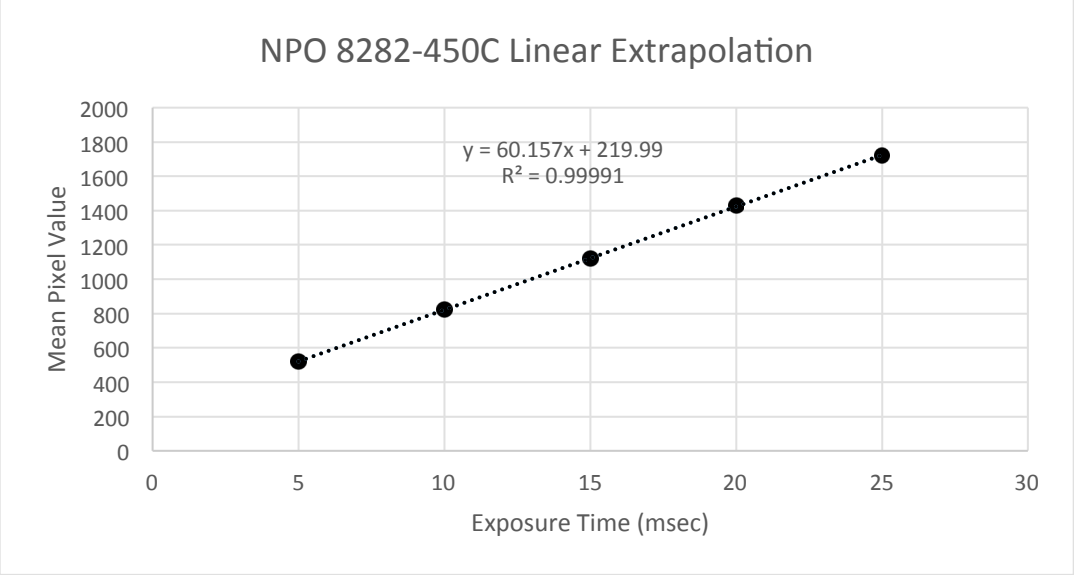

Figure S1. Trend line used for the linear extrapolation of mean pixel intensity values for fluorescence enhancement measurements for Ag-NPO 8282-450C. Sample surface was coated with a PMSSQ film doped to a concentration of 10uM of Rhodamine 6G dye to act as a gain medium.

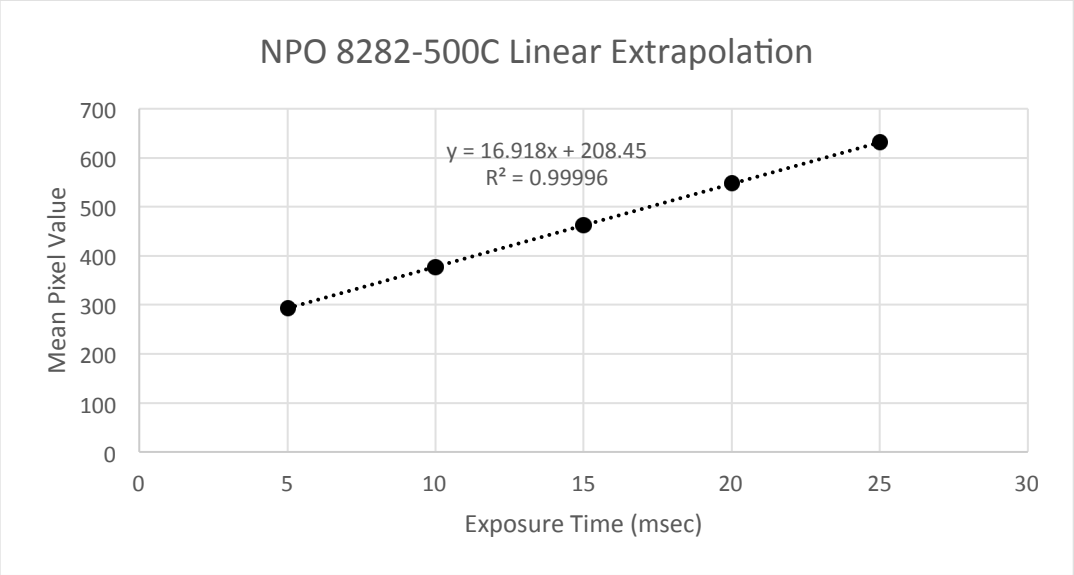

Figure S2. Trend line used for the linear extrapolation of mean pixel intensity values for fluorescence enhancement measurements for Ag-NPO 8282-500C. Sample surface was coated with a PMSSQ film doped to a concentration of 10uM of Rhodamine 6G dye to act as a gain medium.

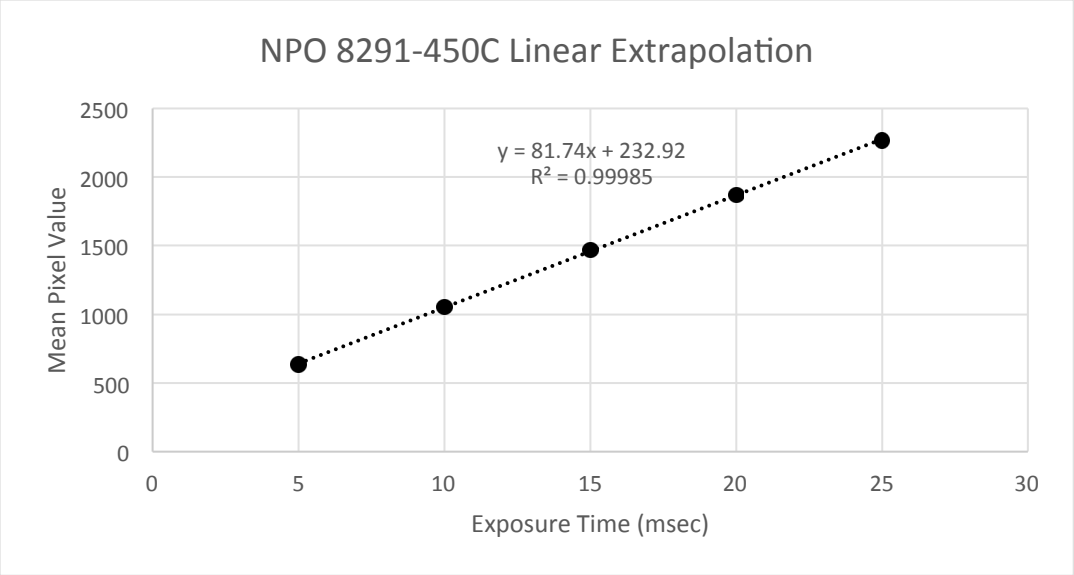

Figure S3. Trend line used for the linear extrapolation of mean pixel intensity values for fluorescence enhancement measurements for Ag-NPO 8291-450C. Sample surface was coated with a PMSSQ film doped to a concentration of 10uM of Rhodamine 6G dye to act as a gain medium.

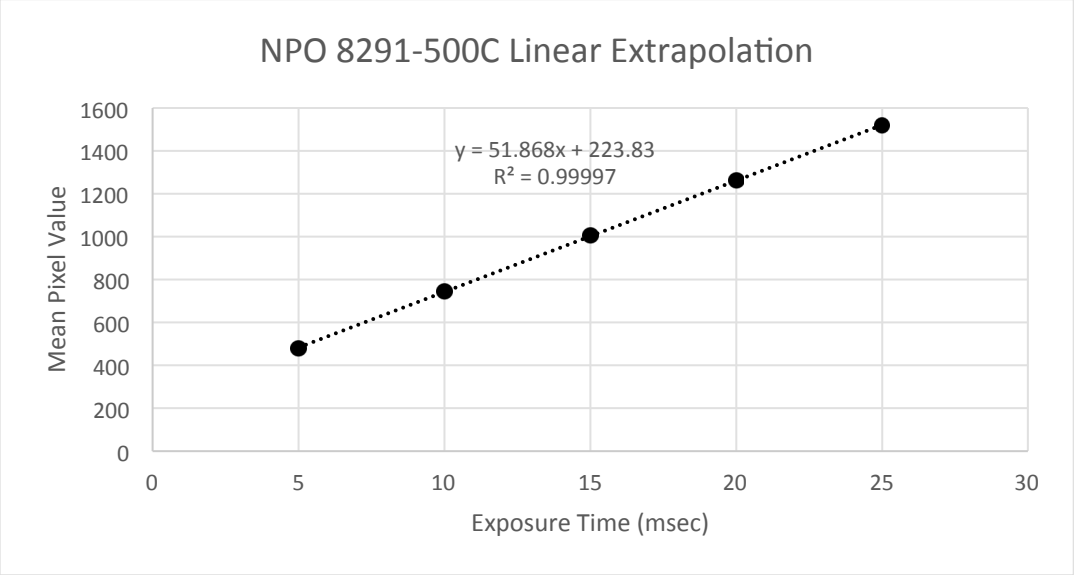

Figure S4. Trend line used for the linear extrapolation of mean pixel intensity values for fluorescence enhancement measurements for Ag-NPO 8291-500C. Sample surface was coated with a PMSSQ film doped to a concentration of 10uM of Rhodamine 6G dye to act as a gain medium.

II. UV-Visible absorption study of the various films.

We captured UV-Visible absorbance spectra of the samples shown in Figure 6 using a Lambda 35 UV-VIS Spectrometer (PerkinElmer, Inc.) The system was set to scan from 400 to 800nm in 1nm increments. Prior to measuring the samples a 100% or 0 Absorbance Baseline Correction was run using a titanium dioxide target. The captured spectra re shown in Figure S5.

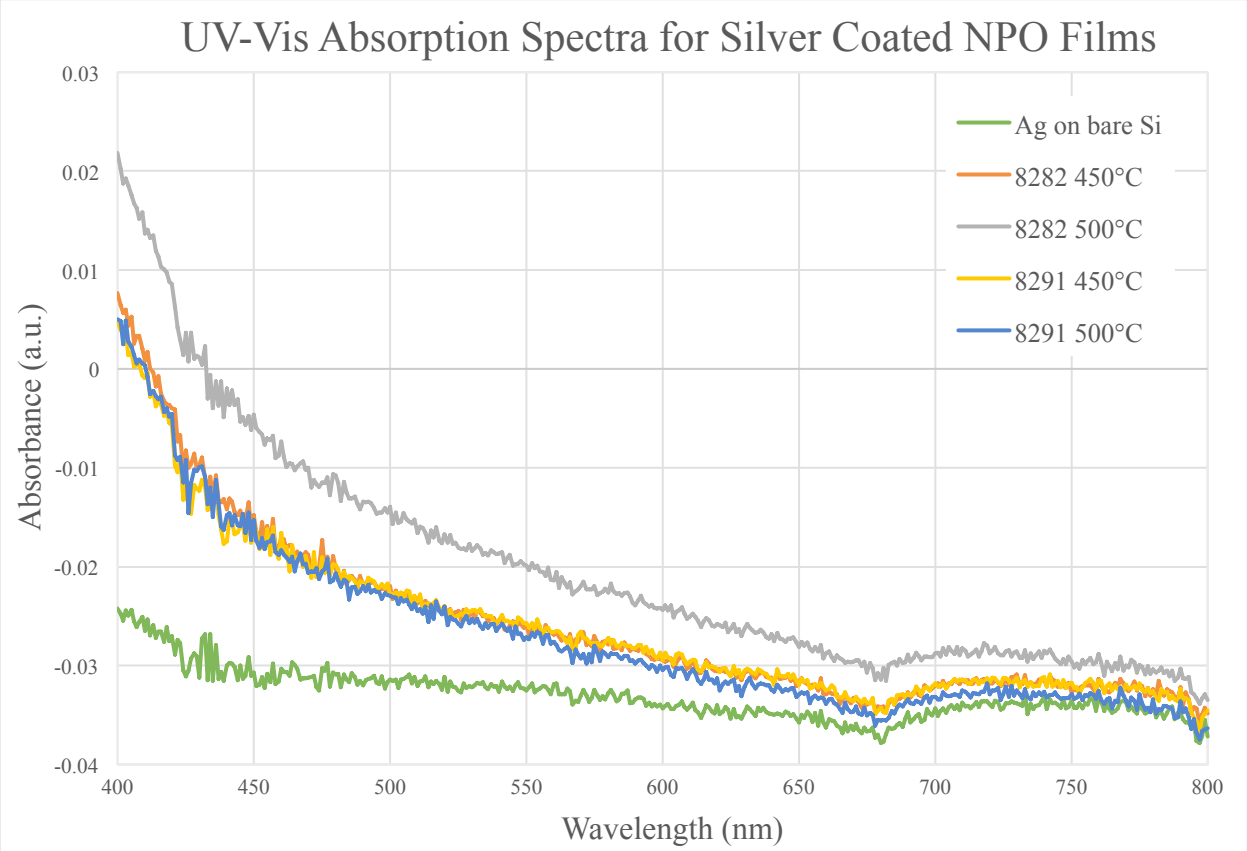

Figure S5. UV-Visible absorption spectra of the various silver nanostructures on NPO.

As expected, the UV-Vis curves indicated very low absorption (as the films were highly reflective, reflectivity close to silver film on bare silicon) across most of the visible spectrum. This further supports our claim that our silver structures are suitable for broad band fluorescence amplification wherein the field enhancement comes both from the nanogaps between the grain structures as well as the fact that these nanogaps serve to launch surface plasmon polaritons in the flat silver grains.

III. FDTD simulation procedure and the parameters

The goal of this experiment was to demonstrate through modelling that the slit defects within silver films similar to the ones obtained for our samples described in the manuscript were capable of coupling free space light photons into propagating surface plasmons within the silver film. Electromagnetic field simulations were performed using Finite Difference Time Domain (FDTD) solutions of the Maxwell's equations using the commercially available software package – Lumerical Solutions. Our structure used for the simulation essentially consisted of an infinite silver film with a single slit defect - 30nm wide and 50nm deep. The corners of the slit were chamfered to approximate it to the experimentally realized slit structures. Note that perfect and sharp slit edges, while experimentally hard to realize also result in highly localized electric dipoles affecting the slit throughput [1]. While the simulated structures are a gross simplification of the actual experimentally realized structures, a superimposition of the field profiles obtained for a number of such simulations with different slit dimensions and their orientations, and grain dimensions nevertheless would converge to the field profiles established over the actual structure.

Table S1: Simulation parameters used in the study

Gap width	30nm
Gap height	50nm
Wavelength Range	350 to 750 nm in 50 nm increments
Source angle (wavelength sweep)	-10 degrees
Distance from source to substrate	325nm
Substrate dimensions	100nm by 10um
FDTD boundaries	PML
Plane wave type	Bloch/periodic
Mesh refinement	Conformal variant 1
Mesh override	0.5nm
Simulation area	X = 1000nm, Y = 600nm
Movie Monitor component	electric field intensity

Table S1 summarizes the parameters used for the simulation. For these simulations, silver was modelled using Johnson and Christy parameters. To illustrate that the slit defects are capable of coupling broadband light to plasmons and at multiple incident angles, two experiments were performed. The first was a wavelength sweep consisting of 5 data points from 450nm to 650nm in 50 nm increments at an angle of incidence of -10 degrees (10 degrees to the left in the

diagram). The second experiment was a sweep of the angle of incidence from 0 degrees to 40 degrees, in 10 degree increments at a wavelength of 545nm (the center frequency of the filter used). Both of the experiments had a substrate of 100nm by 10um. The plane wave source was placed 325nm from the substrate. All of the FDTD boundaries used in the simulation were Perfectly matched layers (PML) to eliminate unwarranted reflections from the boundary. The entire simulation area was 100nm by 600nm and the gap area had a mesh cell size of 0.5nm to improve the accuracy of simulation. Movie monitors were created for each of the points in the two sweeps and these monitors displayed the instantaneous electric field intensities established over the structure as a function of time. Videos showing the evolution of the fields within the nanogap regions as well as the propagating fields established over the plane silver film through slit coupling have been included.

Table S2. List of supplementary video files from the FDTD simulations

Filename	**Angle of Incidence (deg)**	**Wavelength (nm)**
AofI_00_Wavelength_545.mpg	0	545
AofI_10_Wavelength_545.mpg	10	545
AofI_20_Wavelength_545.mpg	20	545
AofI_30_Wavelength_545.mpg	30	545
AofI_40_Wavelength_545.mpg	40	545
Wavelength_450_AofI_10.mpg	450	-10
Wavelength_500_AofI_10.mpg	500	-10
Wavelength_550_AofI_10.mpg	550	-10
Wavelength_600_AofI_10.mpg	600	-10
Wavelength_650_AofI_10.mpg	650	-10

References Cited.

1. Mehfuz, R., Maqsood, M. W., and Chau, K. J. "**Enhancing the Efficiency of Slit-Coupling to Surface-Plasmon-Polaritons via Dispersion Engineering**" *Optics Express* 18, no. 17 (2010): 18206–18216. doi:10.1364/OE.18.018206

IV. Fluorescence Blinking Video Background Information

The supplementary video (Fluorescence_Blinking.avi) shows the hotspot blinking activity seen when imaging the Ag-NPO samples using an epifluorescent microscope (Nikon Eclipse E600 fitted with a Hamamatsu ORCA-ER 12bit CCD camera). The sample in the video is Ag-NPO 8291-450C. Rhodamine 6G dye in Ethanol was incubated until dry on the sample surface prior to imaging. The dye in the solution was at a 0.01uM concentration. 5 uL of solution was dispersed onto a $5mm^2$ are of sample surface. A TRITC-HYQ (530-560 nm ex., 590-650 nm em.) filter cube was used to filter the incident and emitted light. Incident source was a 100 Watt mercury vapor lamp. The video shown was captured using a 100X magnification objective (100x/1.30)

with very low fluorescing immersion oil. Image capture in the camera software was set to a gain of 50 and an exposure time of 100msec. The image area has been reduced by 50% from its original size to reduce the file size.